JOURNAL OF MATERIALS SCIENCE **36** (2001) 1685–1693

Nondestructive evaluation of thermal stress-induced damage in thin composite laminates

NAK-SAM CHOI
Department of Mechanical Engineering, Hanyang University, Ansan 425-791, Korea
SUNG-HYUK LEE
Department of Mechanical Design, Hanyang University, Seoul 133-791, Korea

Nondestructive evaluation of thermal stress-induced failure in the free edge region of thin composite laminates (1 mm thick) has been carried out. The damage zone which arose under a cryogenic cooling was examined using the ultrasonic C-scan and optical microscopy. Characteristic behavior of thermo-acoustic emission (AE) detected from the composite specimen during the heating and cooling cycle indicated the degree of damage which had occurred differently for as-moulded and cryogenically-treated specimens with various lay-up angles. Analysis of the vibration spectrum data obtained with short beam specimens exhibited that the failure occurrence caused an obvious decrease in resonant frequency and some considerable increase in flexural damping ratio. Total AE energy showed a feature similar to the flexural damping ratio which increased with increasing crack density. Consequently, it is thought that thermo-acoustic emission in association with flexural damping might be employed as a tool for nondestructive evaluation of thin composite laminates.

1. Introduction

Recently, fiber-reinforced composite materials have been applied to a variety of components for light-weight structures due to their advantages of superior strength-to-weight and stiffness-to-weight in comparison to metals and alloys. However, damages and flaws may occur during the manufacturing process as well as under in-use conditions, which reduce the mechanical properties, the reliability and the safety of composite structures. Therefore many studies on the nondestructive evaluation of the damage associated with the mechanical property degradation have been reported.

For example, Tracy and Pardeon [1] studied the influence of delamination on the natural frequency of the simply supported composite laminates as a function of stacking sequences using the experimental modal analysis and finite element method. A feasibility study on the vibration spectrum analysis as a tool for nondestructive evaluation of polymer composites was performed by Shelby *et al*. [2]. Shen and Grady [3] proposed a variational method for analyzing the effect of delamination on natural frequency and mode shape of the laminated beam. Penn *et al*. [4] studied the natural frequency of thick composites by the free vibration test using the piezoelectric patches to compare with a finite element analysis result.

Because material state and fracture mechanisms might be estimated by analyzing acoustic emission (AE) data [5–7], the AE measurement technique has been also used for nondestructive evaluation in many engineering fields. The technique has been applied by Sato *et al*. [8] to the composites when they are subjected to a thermal load cycle. Thermo-AE was hardly observed for the composites without damage. However numerous thermo-acoustic emissions were detected for the composites containing damage induced by such mechanical loads as fatigue and static/dynamic loads, which was thus anticipated as a nondestructive evaluation technique for damaged composites.

On the other hand, composite materials are often subjected to external temperature variation when they are applied to structures in the fields of aerospace industry, atomic reactors and electronic parts. For thick composite laminates with thicknesses beyond 3.0 mm, the delamination phenomena caused by thermal stresses were studied by Griffin and Robert [9], Hong and Im [10].

In this paper, thermal stress-induced failures in the free edge region of thin cross-ply $[0_2/90_2]_S$ and angle-ply $[+45_2/-45_2]_S$ laminates (1 mm thick) are studied using thermo-AE measurement and flexural vibration test to find the feasibility of nondestructive evaluation.

2. Experimental

2.1. Composite laminate manufacturing and cryogenic cooling

Composite laminates used for this study were made using a unidirectional carbon fiber/epoxy prepreg (Hankuk Fiber Co.) in autoclave with a curing cycle as in Fig. 1. A temperature drop (ΔT_1) was performed from curing (170 °C) to room temperature. The

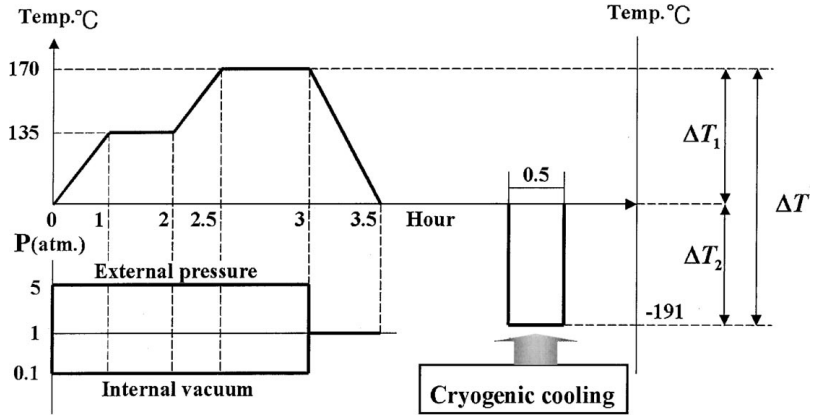

Figure 1 Curing cycle for composite plate manufacturing and cryogenic cooling condition.

manufactured composite laminates 330 mm in length, 215 mm in width and 1 mm in thickness had lay-up angles of $[0_2/+90_2]_S$ and $[+45_2/-45_2]_S$. Square type specimens (80 mm × 80 mm × 1 mm) for cryogenic cooling were made using a diamond wheel cutter. The specimens were completely inserted in the cryogenic chamber (−191 °C) filled with liquid nitrogen for 30 minutes.

2.2. Ultrasonic C-scan

Ultrasonic A-scan was performed in advance of the ultrasonic C-scan. A-scan can detect damages by monitoring reflected waves from the internal defect plane in the specimen. Since the amplitude of reflected waves from the bottom surface (back echo amplitude) could be low due to some amount of reflection at the internal defects, scanning of the back echo amplitude was performed on the specimen by placing the ultrasonic focal point at a constant depth near the upper surface. The ultrasonic transducer was of a focusing type emitting a longitudinal wave of 15 MHz. Its scanning distance and focusing area were 0.085 mm and 0.1 mm, respectively.

2.3. Microscopic fractography

Specimens for microscopic observation were extracted from the edge region of the square type specimens by a diamond wheel cutter. Some damaged region induced by cutting was eliminated by rough polishing. The specimens were molded and a flat polishing was performed with a diamond polishing compound. Microstructure and failures of the specimens were observed using a reflection optical microscope.

2.4. Thermo-acoustic emission measurement

Thermo-acoustic emission was measured by an apparatus consisting of an electric furnace, a wave guide and an acoustic emission measuring system (Mistras-2001, Physical Acoustic Corp.), similarly to what Sato *et al*. [8] did. The specimen of which geometry is shown in Fig. 2b was mounted on one end of a wave guide beam in the furnace by using a vacuum silicone grease and AE transducer(R15, Duengan Corp.: detectable frequency range 100–450 kHz, resonant frequency 150 kHz) was mounted on the other end of the guide beam.

A specimen in the furnace was heated from room temperature to 150 °C at a rate of +4.3 °C/min and then cooled to room temperature at a similar rate. The AE measurement conditions were as follows: Pre-amplification 40 dB, threshold level 35 dB. Acoustic emission energy rate, event count rate and amplitude distribution were obtained in this measurement.

2.5. Flexural vibration test

For flexural vibration testing in the specimen thickness direction, two kinds of specimens (5 mm in width, 1 mm in thickness) with different lengths of 80 mm and 50 mm (see Fig. 2c) were extracted from the edge region of the C-scanned specimens using the diamond wheel cutter. During the vibration sweep test, one side of the specimen, 15 mm in length, corresponding to the

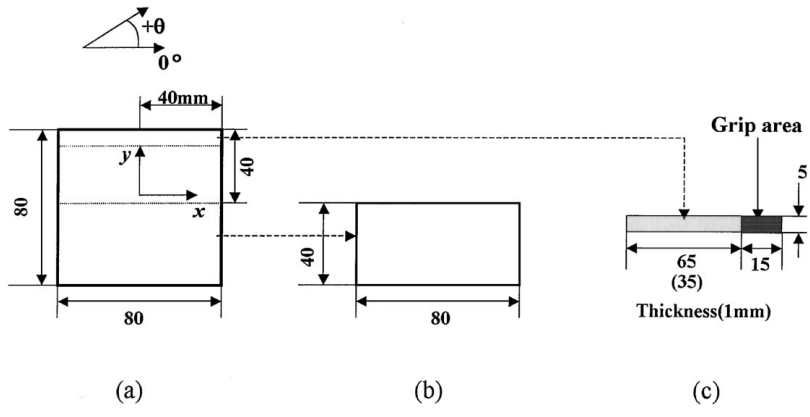

Figure 2 Specimens for (a) cryogenic cooling, (b)thermo-acoustic emission measurement and (c) flexural vibration.

zone where failure was scarcely observed on the basis of the ultrasonic C-scan results, was in a fixed state with a clamping device. The fixed location was excited with a forced sine wave load and the dynamic displacement at the other side of specimen was monitored with a laser micrometer and was then processed with a dynamic signal analyzer to measure frequency response function (FRF).

From the measured FRF for each vibration mode, damping ratios ζ_i are obtained from the equation [13]

$$\zeta_i = \frac{f_b - f_a}{2 f_i} \quad (1)$$

where f_i is resonant frequency for i-th mode; f_a and f_b are the frequencies corresponding to $1/\sqrt{2}$ of the peak amplitude.

3. Results and discussion

3.1. Fracture mechanisms in the free edge region

3.1.1. Ultrasonic C-scan image

Fig. 3 shows a typical result of the C-scan obtained from a $[0_2/90_2]_S$ laminate experienced by liquid nitrogen immersion. The x-axis indicates the fiber direction in the 0° skin layer. Fig. 3a and b are the scanning result and its illustration, respectively. Area A, in comparison with the corner area B and other areas, exhibited a dark image representing a damage zone which was formed in a region $y = 37$–40 mm near the free edge of the laminate. Thermal stress-induced failure in the $[0_2/+90_2]_S$ laminate took place in the free edge region where the fiber orientation in the core layer was perpendicular to the free section. Although the back-echo amplitude was more or less under the influence of the reflective noise waves at the free edge and/or section, it is to be noted that the image of damage near the free edge could be observed using the focusing-type transducer with a 15 MHz longitudinal emission. On the other hand, such image of damage was hardly observed for as-moulded specimens by the C-scan.

Fig. 4a shows an ultrasonic C-scan result of a $[45_2/-45_2]_S$ laminate subjected to liquid nitrogen immersion. The corner region C of the laminate revealing a dark image was damaged. Failure formation was distributed in a range about 13 mm from the corner point of the laminate as illustrated in Fig. 4b.

3.1.2. Microscopic observation of cracks

Fig. 5 is an optical micrograph taken from the cross section corresponding to the free edge of the specimen in Fig. 3, showing an interlaminar region between the core layer with 90° fibers and the skin layer with 0° fibers. Micro-cracks occurred in the core layer near the plies interface and propagated through the matrix and the fiber-matrix interface. Average length of the transverse cracks was 540 μm, indicating that a high magnitude of the tensile thermal stresses beyond the fracture stress had occurred during the cryogenic cooling. The direction of the cracks in the $[0_2/90_2]_S$ laminate was in a range of 0°–20° angles with reference to the fiber direction in the 0° layer. It is thought that the crack angle depended on the ratio of the interlaminar normal stress σ_z to the in-plane normal stress σ_x [11]. Based on the results of Figs 3 and 5, a schematic of the edge-failure formation of the $[0_2/+90_2]_S$ laminate is shown in Fig. 6. Micro-cracks took place in the 90° core layer near the 0°/90° plies interface in the free edge region and propagated about 3 mm in depth. No cracks were seen in the skin layer. Fig. 7 is an optical micrograph taken from the section in the corner region C of the specimen in Fig. 4. Cracks took place in the core layer with −45° fibers near the +45°/−45° plies interface.

Table I summarizes average crack length, crack density (total crack length per core layer sectional area), damage zone size l_c and crack angle for each laminate obtained from the above failure observation and

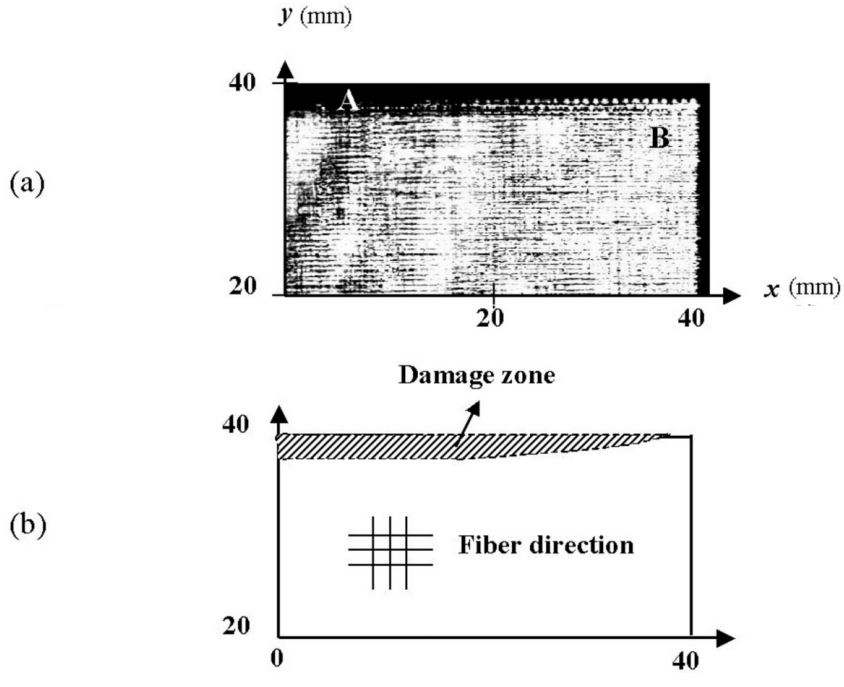

Figure 3 Ultrasonic C-scan result of a $[0_2/+90_2]_S$ laminate treated by liquid nitrogen immersion.

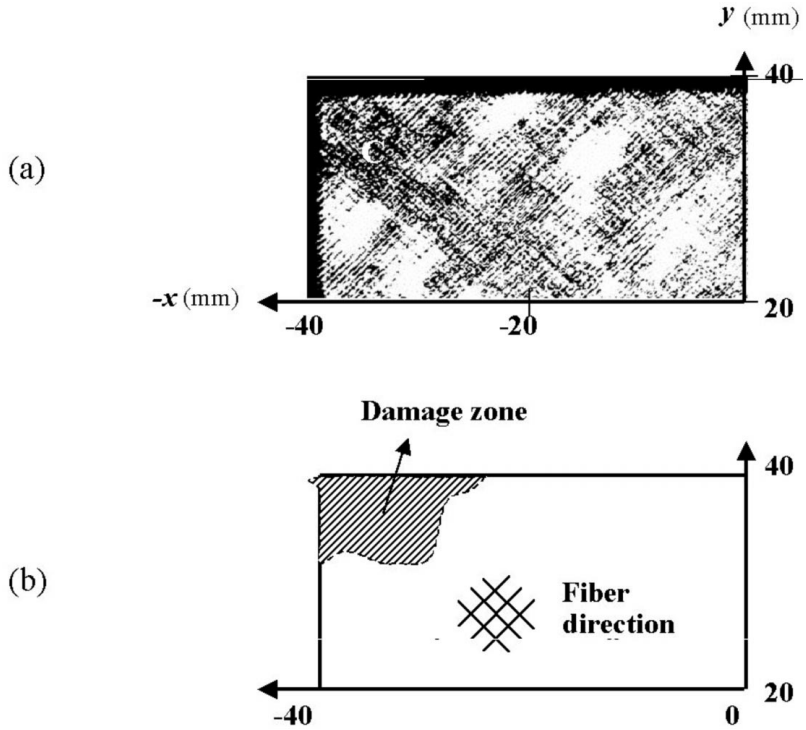

Figure 4 Ultrasonic C-scan result of a $[+45_2/-45_2]_S$ laminate treated by liquid nitrogen immersion.

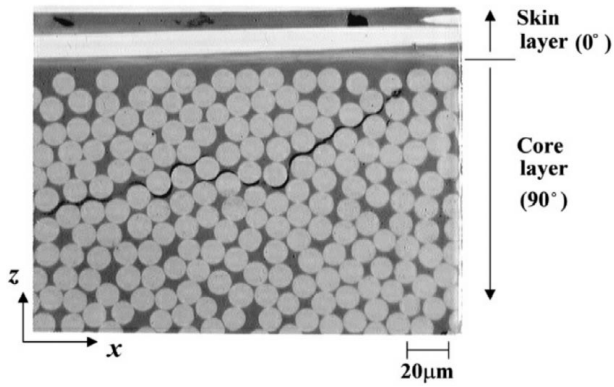

Figure 5 Optical micrograph taken from the cross-section near the free edge of a $[0_2/+90_2]_S$ laminate.

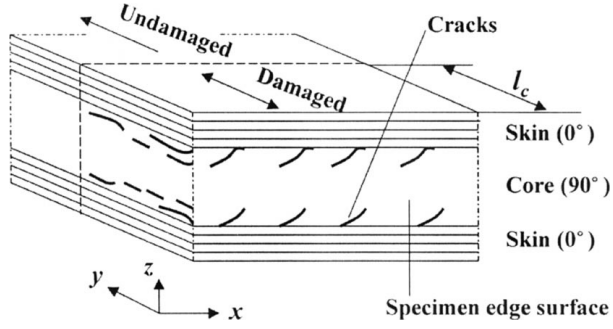

Figure 6 Schematic of the edge-failure occurrence of $[0_2/+90_2]_S$ composite laminate.

the ultrasonic C-scan. Crack length and crack density of the $[0_2/90_2]_S$ laminate were larger than those of the $[+45_2/-45_2]_S$ laminate, while the damage zone in the $[+45_2/-45_2]_S$ laminate was deeper. Many cracks arose in the core layer under the cryogenic cooling, while only a few cracks were observed for the specimens subjected to cooling to room temperature.

TABLE I Edge-failure data obtained from as-moulded(A: 23°C) and cryogenically cooled (B: −191°C) specimens

	Specimen	Crack length (μm)	Crack density ($\times 10^{-4}\mu m^{-1}$)	Damaged zone l_C (mm)	Crack angle (°)
A	$[0_2/+90_2]_S$	160	16.46	-	-
	$[+45_2/-45_2]_S$	190	7.84	-	-
B	$[0_2/+90_2]_S$	540	21.2	3	0∼20
	$[+45_2/-45_2]_S$	420	16.5	13	15∼45

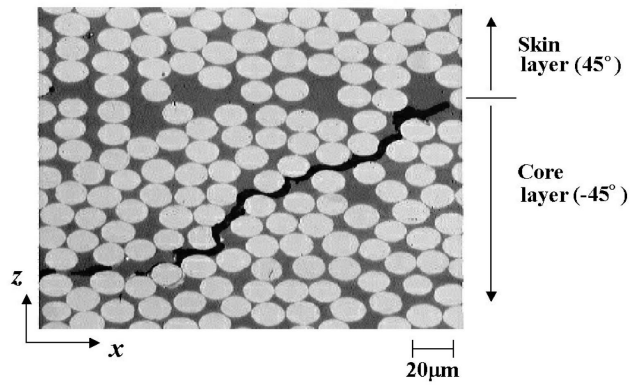

Figure 7 Optical micrograph taken from the cross-section near the free edge of a $[+45_2/-45_2]_S$ laminate.

3.1.3. Thermal stress distribution

The three dimensional finite element program ANSYS 5.3 was used to predict thermal stress distribution in $[0_2/+90_2]_S$ and $[+45_2/-45_2]_S$ carbon/epoxy laminates under the cryogenic condition. The geometry and material properties of the laminate model for the finite element analysis were adopted similar to those of the specimen shown in Fig. 2a. The model was cooled from the stress-free to the room temperature ($\Delta T = -100\,^{\circ}$C).

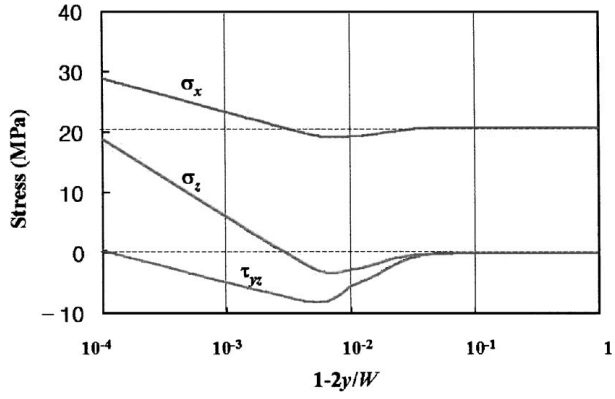

Figure 8 In-plane σ_x and interlaminar stresses σ_z, τ_{yz} in the 90° layer near the ply-interface of a $[0_2/+90_2]_S$ laminate.

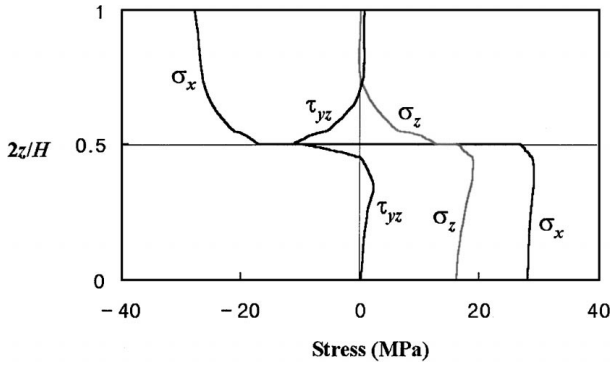

Figure 9 Through-thickness distribution of edge stresses at the free edge of a $[0_2/+90_2]_S$ laminate.

Fig. 8 shows distribution of in-plane (σ_x) and interlaminar stresses (σ_z, τ_{yz}) along the y-axis in the 90° core layer near the ply-interface ($z = H/4$) of a $[0_2/90_2]_S$ laminate (length $L =$ width $W = 80$ mm, thickness $H = 1$ mm) which may influence the generation of micro-cracks. The left end of the horizontal axis in this figure corresponds to the free edge where the micro-cracks were observed by the ultrasonic C-scan and optical microscopy. As compared with the constant value of stress (a dotted line in Fig. 8) predicted by the classical laminated plate theory, the stresses near the edge exhibited a large increase in a tensile mode. Fig. 9 presents through-thickness distribution of the stresses at the free edge ($x = 0$, $y = 40$ mm) of the $[0_2/90_2]_S$ laminate. $2z/H = 0$ corresponds to the symmetric center plane of the core layer and $2z/H = 1$ corresponds to the upper surface of the skin layer. A stress singularity exists at the 0°/90° ply interface ($2z/H = 0.5$) on account of the mismatch in material properties between the plies. The values of σ_z and τ_{yz} converged to zero near the upper surface of the skin layer, whereas σ_x and σ_z revealed large values of tensile stresses in the core layer with 90° orientation.

The thermal stress σ has a linear relationship with temperature difference ΔT, given by

$$\sigma = f(\alpha, E)\Delta T \tag{2}$$

where α and E are the thermal expansion coefficient and the elastic modulus depending on the fiber direction. Values of stresses arising at any temperature drop can be determined by multiplication of the stress values with a normalized value of temperature difference $\Delta T/100$.

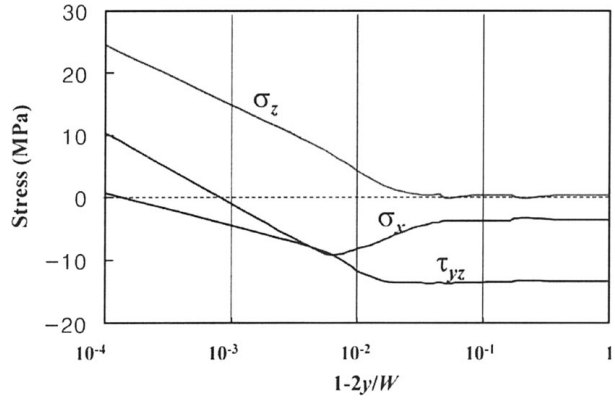

Figure 10 In-plane σ_x and interlaminar stresses σ_z, τ_{yz} in the −45° layer near the ply-interface of a $[+45_2/-45_2]_S$ laminate.

Combinations of thermal in-plane stress σ_x and interlaminar stress σ_z caused the formation of cracks in the free edge region shown in Figs 3 and 5 when the specimen suffered the cryogenic cooling ($\Delta T/100 = -3.1$).

Stress distribution near the corner ($z = 0.88H/4$, $x = -40$ mm) for the $[+45_2/-45_2]_S$ laminate is shown in Fig. 10. The closer to the left end ($x = -40$ mm, $y = 40$ mm) of the horizontal axis, the bigger in σ_x and σ_z. This corresponded to the occurrence of failure in the corner region shown in Figs 4 and 6. The calculation result that the ratio of σ_z/σ_x at the left end was bigger than that of Fig. 8 agreed with the experimental one that the crack angle of the $[+45_2/-45_2]_S$ laminate was larger than that of the $[0_2/90_2]_S$ laminate.

3.2. Thermo-acoustic emission behavior

For understanding thermo-acoustic emission (AE) sources in the laminates, a thick $[45_6/-45_6]_S$ specimen having a similar lay-up structure and a thickness of about 3 mm was adopted because thicker laminates were expected to suffer more failure by the cryogenic treatment [11] and thus generation of many thermo-AE event-counts was expected from the damaged region. Fig. 11 shows behaviors of thermo-AE event-count rates measured from the specimen with liquid nitrogen treatment during the repetative thermal cycles. During the first thermal cycle shown in Fig. 11a, large values of the AE event-count rate were obtained. However, it drastically decreased in the second thermal cycle (Fig. 11b). This may indicate that cracking did not proceed further when the specimen was subjected to the thermal cycles. Sources of this thermo-AE may have come from some friction between crack surfaces being moved by thermal deformation mismatch between the plies as well as by relaxation of residual stresses accumulated around the crack under the thermal cycles.

Behaviors of AE energy rate from untreated and cryogenically treated $[0_2/90_2]_S$ thin specimens with a thickness of 1 mm are shown in Fig. 12a and b, respectively. Thermo-AE was intermittently generated from the untreated laminate, which indicates that a limited amount of failure might have occurred in the free edge region of the laminate due to the temperature drop from curing to room temperature. Compared with the untreated case,

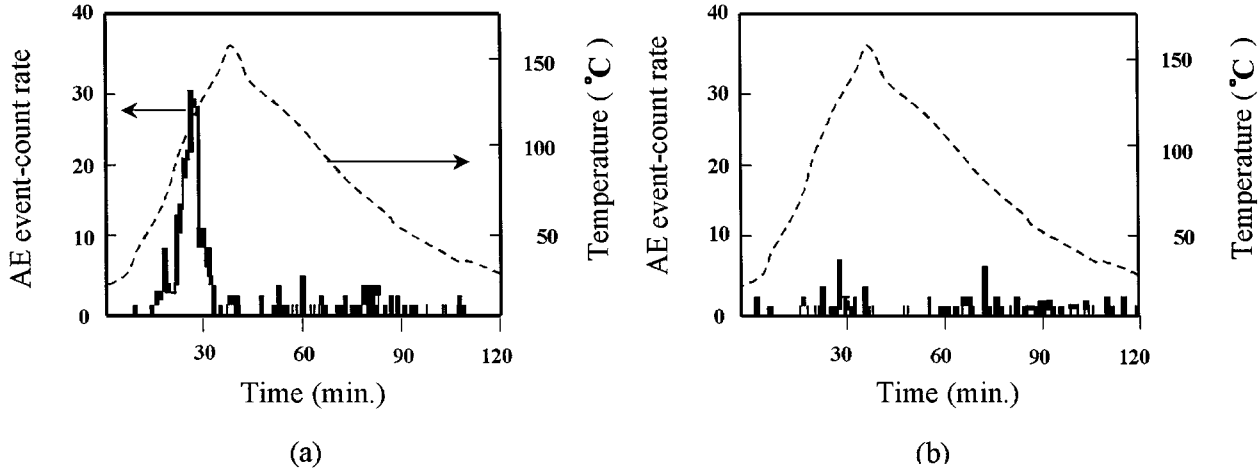

Figure 11 Thermo-acoustic emission behavior of a $[+45_6/-45_6]_S$ specimen during (a) the 1st and (b) 2nd heating and cooling cycles.

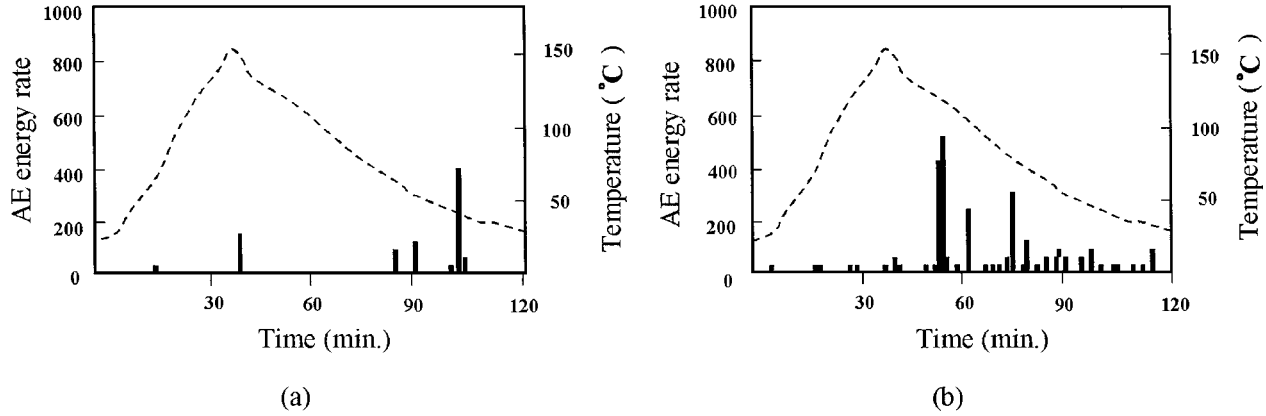

Figure 12 Characteristic behaviors of thermo-AE energy rate measured form (a) untreated and (b) cryogenically treated $[0_2/+90_2]_S$ laminates.

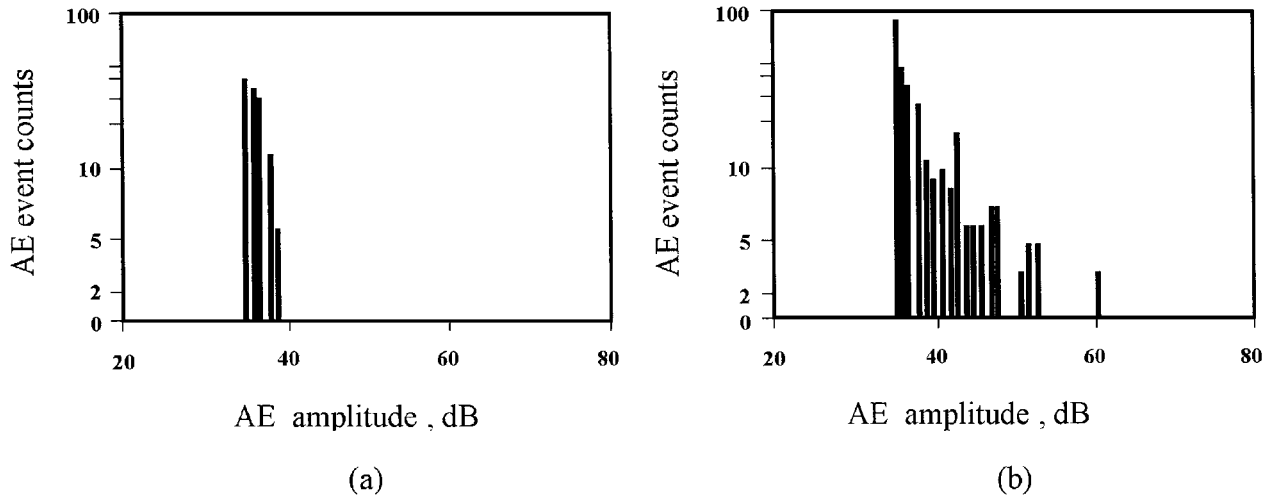

Figure 13 AE event-counts versus peak amplitude distribution of (a) untreated and (b) cryogenically treated $[0_2/+90_2]_S$ laminates.

the average value of the AE energy rate measured from cryogenically treated laminate was about 3 times larger during the thermal cycle. Diagrams of AE event-counts versus peak amplitude distribution, corresponding to Fig. 12a and b, are shown in Fig. 13a and b, respectively. Strong emissions with amplitudes up to 60 dB were generated in the treated specimens, while emissions from the untreated specimen had low amplitudes below 40 dB. This agreed with the C-scan results (see Figs 3, 4 and Table I) in that cracks arose with large density in the free edge region of the $[0_2/90_2]_S$ laminates affected by cryogenic cooling. Similar AE amplitude features were observed for untreated and cryogenically treated $[+45_2/-45_2]_S$ specimens (see Fig. 14a and b), except that somewhat weak amplitude emissions were produced.

3.3. Flexural vibration characteristics

3.3.1. Resonant frequency change with failure formation

Fig. 15 shows a typical frequency response function (FRF) curve of the first mode measured from a

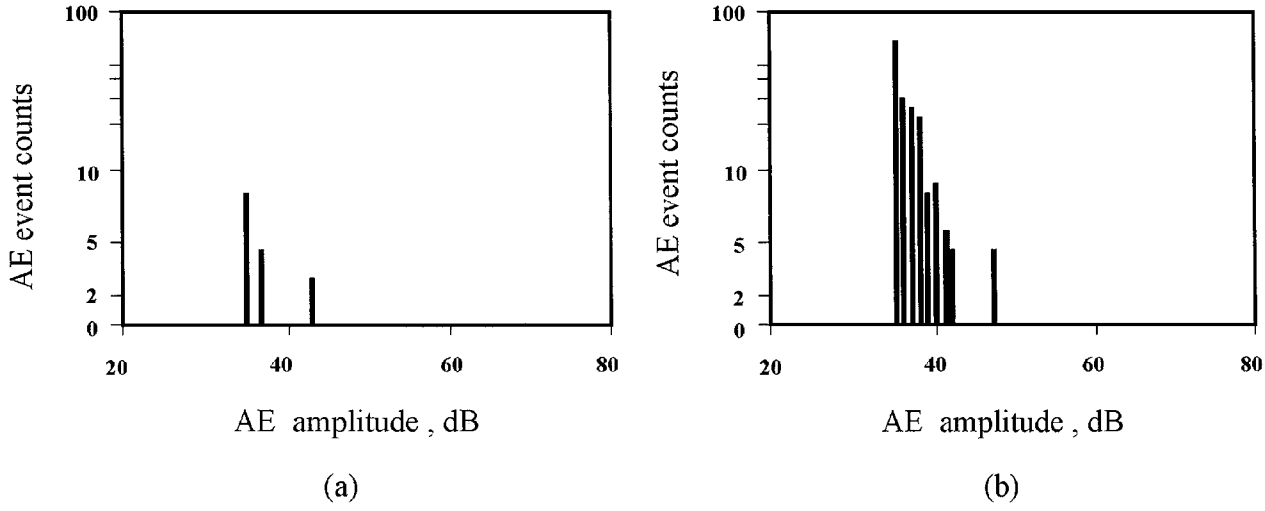

Figure 14 AE event-counts versus peak amplitude distribution of (a) untreated and (b) cryogenically treated $[+45_2/-45_2]_S$ laminates.

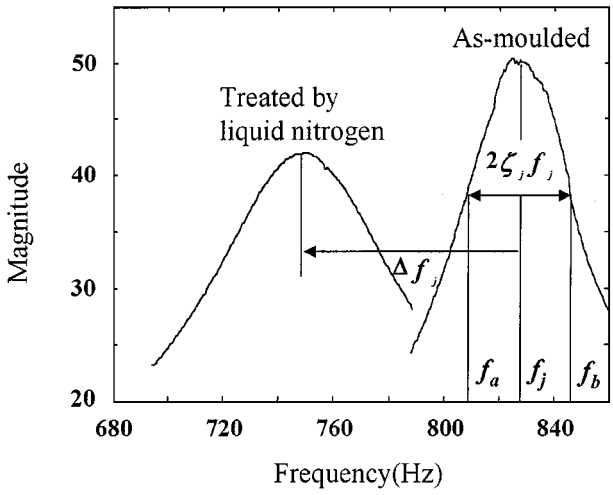

Figure 15 Frequency response curves measured from as-moulded and cryogenically treated $[0_2/+90_2]_S$ specimens.

$[0_2/90_2]_S$ specimen with a geometry (effective specimen length 35 mm) of Fig. 2b containing the damage zone in Fig. 3. For comparison, the other curve obtained from a specimen in an as-moulded state is shown in the same Figure. It is to be noted that the resonant frequency of the specimen decreased as much as $\Delta f_i \fallingdotseq 80$ Hz due to the existence of micro-cracks smaller than 0.5 mm and, in addition, the width ($f_b - f_a$) of the FRF curve representing the damping ratio ζ_i was considerably enlarged. This indicates that the FRF characteristics may be utilized for nondestructive evaluation of the present thin composite laminates which is compared with the studies [1–4] utilizing the thick composite laminates containing delamination larger than 2 mm.

Table II lists the resonant frequency data of the first and second modes. Since flexural stiffness of the $[+45_2/-45_2]_S$ specimens was lower than that of the $[0_2/90_2]_S$ specimens, resonant frequencies for the $[+45_2/-45_2]_S$ specimens at each mode decreased to only 40% of that for the $[0_2/90_2]_S$ specimens. In case of the damaged $[0_2/90_2]_S$ specimens, resonant frequencies showed a definite decrease at both the modes and were much more lessened for shorter specimens. This drop in resonant frequencies arose due to the decrease in flexural stiffness caused by crack occurrence. For the damaged $[+45_2/-45_2]_S$ specimens, resonant frequency scarcely changed at the first mode, and slightly decreased at the second mode. The reasons for the decreased sensitivity of resonant frequency were thought to be that the damage zone of the $[+45_2/-45_2]_S$ specimens was formed only in a local region (length 13 mm) around the corner and thus the number of micro-cracks was much less than that for the $[0_2/90_2]_S$ specimens.

3.3.2. Damping ratio change with failure formation

Table III presents values of the first and second mode damping ratio ζi measured through Equation 1. In the case of the effective specimen length 65 mm, damping ratio was not so influenced by the cryogenic cooling. In the case of 35 mm length, damping ratio considerably increased at both the modes for the $[0_2/90_2]_S$ specimens and at the first mode for the $[+45_2/-45_2]_S$. The increase in vibration damping might be caused by the friction between crack surfaces. The large values of damping ratio in the short beam specimens are understandable with a view point of the structural mechanics

TABLE II Resonant frequency f_i of flexural specimens(A: as-moulded, B: cryogenically cooled)

Mode	Effective specimen length (mm)	$[0_2/+90_2]_S$			$[+45_2/-45_2]_S$		
		f_A (Hz)	f_B (Hz)	$f_B - f_A$	f_A (Hz)	f_B (Hz)	$f_B - f_A$
1	35	$827.9^{+19.9}_{-19.9}$	$747.8^{+22.3}_{-22.3}$	−80.1	$348.7^{+9.5}_{-11.6}$	$343.7^{+6.1}_{-11.2}$	−5.0
	65	212.5^{+6}_{-6}	$200.3^{+7.8}_{-7.8}$	−15.2	$91.3^{+0.8}_{-0.8}$	$86.8^{+2.0}_{-2.0}$	−4.5
2	35	$5515.7^{+122.5}_{-122.5}$	$5112.5^{+98.5}_{-98.5}$	−401.2	$2378.7^{+42.5}_{-32.5}$	$2331.3^{+51.2}_{-27.5}$	−47.4
	65	$1374.0^{+29.8}_{-29.8}$	$1267.2^{+27.5}_{-27.5}$	−106.8	$568.9^{+2.6}_{-2.6}$	$553.1^{+7.7}_{-7.7}$	−15.8

TABLE III Damping ratio ζ_i of flexural specimens(A: as-moulded, B: cryogenically cooled)

Mode	Effective specimen length (mm)	$[0_2/+90_2]_S$			$[+45_2/-45_2]_S$		
		$\zeta_A(\times10^{-3})$	$\zeta_B(\times10^{-3})$	$\zeta_B-\zeta_A$	$\zeta_A(\times10^{-3})$	$\zeta_B(\times10^{-3})$	$\zeta_B-\zeta_A$
1	35	$15.0^{+5.7}_{-5.7}$	$33.2^{+6.2}_{-6.2}$	+18.2	$7.0^{+2.1}_{-1.9}$	$12.9^{+8.6}_{-4.5}$	+5.9
	65	$3.4^{+0.1}_{-0.1}$	$3.2^{+1.2}_{-1.2}$	−0.2	$2.5^{+0.2}_{-0.1}$	$2.7^{+0.5}_{-0.3}$	+0.2
2	35	$12.8^{+3.2}_{-3.2}$	$14.2^{+2.5}_{-2.5}$	+1.4	$41.0^{+8.0}_{-8.0}$	$32.0^{+6.0}_{-6.0}$	−9.0
	65	$12.7^{+4.3}_{-4.3}$	$12.6^{+5.2}_{-5.2}$	−0.1	$5.0^{+0.9}_{-0.4}$	$5.3^{+1.5}_{-1.3}$	+0.3

[12] in that large shearing stresses can be produced in the interior of short beam during flexural deformation in vibration, inducing much frictional sliding between crack surfaces.

3.4. Acoustic emission energy and flexural damping versus crack density

Fig. 16 shows values of total AE energy and flexural damping ratio measured as a function of crack density for $[0_2/90_2]_S$ specimens. Low and high values of crack density were obtained from the as-moulded and cryogenically cooled specimens, respectively. Both AE energy and flexural damping increased with increasing crack density. High crack density represents large value in total area of cracks, which seemed to cause AE energy and flexural damping to be large. This is understandable on the assumption that thermo-acoustic emission was generated from friction between crack surfaces which was the dominant factor of the flexural damping. Similar results were obtained for $[+45_2/-45_2]_S$ specimens as shown in Fig. 17, except that values of AE energy and flexural damping were comparatively low. Thus, thermo-acoustic emission in association with flexural damping might be expected as a tool for nondestructive evaluation of thin composite laminates.

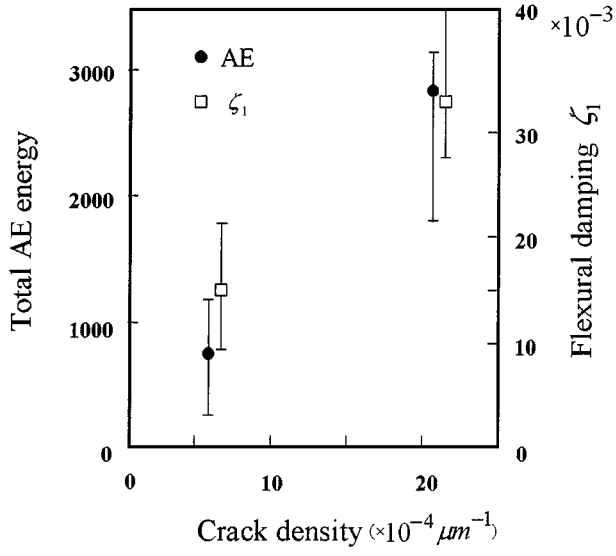

Figure 16 Total AE energy and flexural damping ratio versus crack density for $[0_2/+90_2]_S$ specimens.

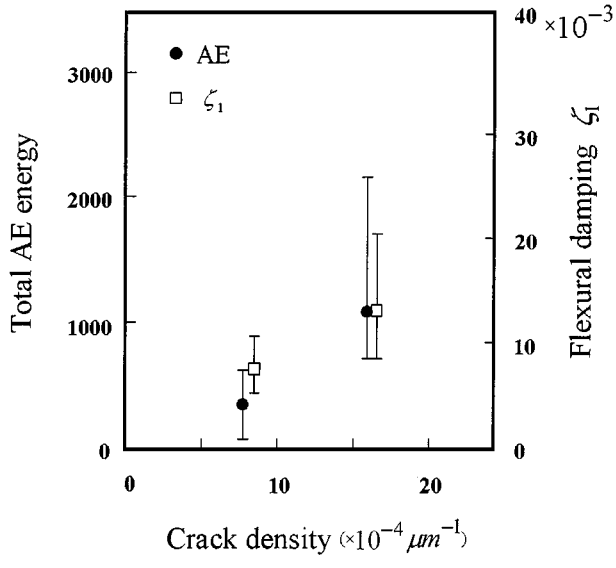

Figure 17 Total AE energy and flexural damping ratio versus crack density for $[+45_2/-45_2]_S$ specimens.

4. Conclusions

Thermal stress-induced failure in the free edge region of thin composite laminates with a thickness of 1 mm has been evaluated employing the thermo-acoustic emission (AE) and flexural vibration methods. The damage zone which was produced under a cryogenic cooling was examined utilizing the ultrasonic C-scan and optical microscopy. Thermo-acoustic emission waves were detected from the composite specimen during the heating and cooling cycle, which estimated the degree of damage different for as-moulded and cryogenically-treated laminates with various lay-up angles. Vibration spectrum data obtained with short beam specimens showed that such failure occurrence led to a decrease in resonant frequency and some considerable increase in flexural damping ratio. The behavior of the flexural damping ratio agreed with the increasing feature of total AE energy with increasing crack density. Thus, it is thought that thermo-AE behaviors as well as the amount of flexural damping depending on friction between crack surfaces might be employed for nondestructive evaluation of thin composite laminates.

References

1. J. J. TRACY and G. C. PARDOEN, *J. Composite Materials* **23** (1989) 1200.
2. M. D. SHELBY, H. J. TAI and B. Z. JANG, *Polymer Engineering and Science* **31** (1991) 47.
3. M.-H. H. SHEN and J. E. GRADY, *AIAA Journal* **30** (1992) 1361.
4. L. S. PENN, J. R. JUMP, M. J. GREENFIELD and G. E. BLANDFORD, *J. Composite Materials* **33** (1999) 54.
5. N. S. CHOI, K. TAKAHASHI and K. HOSHINO, *NDT & E International* **25** (1992) 271.

6. N. S. CHOI and K. TAKAHASHI, *J. Mater. Sci.* **33** (1998) 2357.
7. J. H. KIM, B. W. AHN, J. W. SA and B. J. PARK, *J. of Korean Society for Nondestructive Testing* **19** (1999) 277.
8. N. SATO, T. DURAUCHI and O. DAMIGAITO, *J. Composite Materials* **22** (1988) 447.
9. D. H. GRIFFIN JR. and J. C. ROBERT, *ibid.* **17** (1983) 539.
10. S. G. LIM and C. S. HONG, *KSME Transactions* **11** (1987) 586.
11. S. H. LEE and N. S. CHOI, *J. Korean Society for Composite Materials* **12** (1999) 28.
12. A. C. UGURAL and S. K. FENSTER, "Advanced Strength and Applied Elasticity," 3rd ed. (Prentice Hall PTR, New Jersey, 1995).
13. M. PAZ, "Structural Dynamics: Theory and Computation" (Chapman and Hall, New York, 1997).

Received 3 March
and accepted 17 August 2000